NASA TECHNICAL NOTE

NASA TN D-5409

NASA TN D-5409

ANALYSIS OF THE FLAT-SPIN CHARACTERISTICS OF A TWIN-JET SWEPT-WING FIGHTER AIRPLANE

by Joseph R. Chambers, James S. Bowman, Jr., and Ernie L. Anglin

Langley Research Center
Langley Station, Hampton, Va.

NATIONAL AERONAUTICS AND SPACE ADMINISTRATION • WASHINGTON, D. C. • SEPTEMBER 1969

1. Report No. NASA TN D-5409	2. Government Accession No.	3. Recipient's Catalog No.
4. Title and Subtitle ANALYSIS OF THE FLAT-SPIN CHARACTERISTICS OF A TWIN-JET SWEPT-WING FIGHTER AIRPLANE		5. Report Date September 1969 6. Performing Organization Code
7. Author(s) Joseph R. Chambers, James S. Bowman, Jr., and Ernie L. Anglin		8. Performing Organization Report No. L-6751
9. Performing Organization Name and Address NASA Langley Research Center Hampton, Va. 23365		10. Work Unit No. 126-62-11-01-23 11. Contract or Grant No. 13. Type of Report and Period Covered Technical Note
12. Sponsoring Agency Name and Address National Aeronautics and Space Administration Washington, D.C. 20546		14. Sponsoring Agency Code

15. Supplementary Notes

16. Abstract

An investigation was conducted to determine the significant factors affecting the flat-spin characteristics of a contemporary high-performance fighter airplane having horizontal tail surfaces with negative geometric dihedral (droop). Various phases of the study included static and forced-oscillation wind-tunnel tests, rotary-balance tests, single-degree-of-freedom autorotation tests, and free-spinning tests of a dynamically scaled model.

17. Key Words Suggested by Author(s) Spinning Spin recovery Test techniques	18. Distribution Statement Unclassified – Unlimited		
19. Security Classif. (of this report) Unclassified	20. Security Classif. (of this page) Unclassified	21. No. of Pages 33	22. Price* $3.00

*For sale by the Clearinghouse for Federal Scientific and Technical Information
Springfield, Virginia 22151

ANALYSIS OF THE FLAT-SPIN CHARACTERISTICS OF A TWIN-JET SWEPT-WING FIGHTER AIRPLANE

By Joseph R. Chambers, James S. Bowman, Jr.,
and Ernie L. Anglin
Langley Research Center

SUMMARY

An investigation was conducted to determine the significant factors affecting the flat-spin characteristics of a contemporary high-performance fighter airplane having horizontal tail surfaces with negative geometric dihedral (droop). Various phases of the study included static and forced-oscillation wind-tunnel tests, rotary-balance tests, single-degree-of-freedom autorotation tests, and free-spinning tests of a dynamically scaled model.

The results of the investigation indicated that the fast flat spin exhibited by the airplane was caused by autorotational aerodynamic moments which resulted from interference effects between the vertical tail surface and the drooped horizontal tail surfaces. Several modifications to the basic airplane tail arrangement were designed to eliminate the aerodynamic causes of the flat spin and consequently either eliminate or provide recovery from this type of spin. The most feasible modification for retrofit to production airplanes seemed to be the use of increased trailing-edge-up deflection of the horizontal tail. Spin-tunnel results indicated that use of increased trailing-edge-up deflection of the stabilator together with standard recovery controls (ailerons with, rudder against) and simultaneous deployment of a 16-foot (4.88-m) landing drag parachute (with a distance from the attachment point to the canopy equal to 100 feet (30.48 m)) result in acceptable recovery characteristics from the flat spin.

INTRODUCTION

Perhaps the most dangerous spinning motion exhibited by an airplane is the fast flat spin in which the airplane angle of attack approaches 90° (fuselage approximately horizontal) with attendant high rates of rotation. As the airplane angle of attack approaches 90°, conventional aerodynamic control surfaces become relatively ineffective and recovery from the developed flat spin may therefore become impossible. Recovery from the fast flat spin has always been difficult, but the problem has increased considerably with contemporary fighter airplanes. With the advent of jet engines and sweptback wings the

weight of fighter airplanes has increased much more rapidly than the physical dimensions of the airplanes, and a large part of the overall weight has been spread out along the fuselage. As a result, present-day fighter airplanes have moments of inertia in yaw 20 times as large as fighter airplanes of 20 years ago, whereas the aerodynamic control surfaces, especially the rudder, have not changed significantly in size or moment arm. Consequently, fast flat spins of current fighter airplanes are not easily terminated because of the large increase of angular momentum contained within the spin. As pointed out in reference 1, fast flat spins are usually associated with low aerodynamic damping in yaw at spinning attitudes. In the past, airplane-configuration features such as shielded vertical tail surfaces and fuselage cross-sectional shapes have been identified as factors contributing to the low values of damping in yaw.

The present paper is a summary of results obtained during an investigation to determine the significant factors contributing to a fast flat-spin mode exhibited by a twin-jet swept-wing fighter configuration having horizontal tail surfaces with negative dihedral. Previous experience has shown that recovery from the flat spin is impossible by using normal spin-recovery techniques. A detailed discussion, which describes a series of wind-tunnel tests that identified the principal features of the airplane which caused the flat spin, is presented. Information is also presented regarding the effects of several configuration modifications designed to eliminate the aerodynamic causes of the flat spin and consequently either eliminate or provide recovery from this type of spin. The results of the investigation are meant (1) to indicate possible modifications which might lead to satisfactory recoveries from the fast flat spin of the particular airplane and (2) to provide a better general understanding of the effects of some factors which can cause a flat spin.

SYMBOLS

Aerodynamic quantities are presented with respect to a body system of axes. All data are referred to a center-of-gravity position of 27-percent wing mean aerodynamic chord unless otherwise noted. Dimensional values herein are given in U.S. Customary Units and in the International System of Units.

b wing span, ft (m)

$\bar{c}$ wing mean aerodynamic chord, ft (m)

$\bar{c}_t$ horizontal tail mean aerodynamic chord, ft (m)

C_n yawing-moment coefficient, $\dfrac{M_Z}{\frac{1}{2}\rho V^2 Sb}$

h	vertical location of horizontal tail, ft (m)
i_t	horizontal tail incidence angle, deg
I_X, I_Y, I_Z	moments of inertia about X-, Y-, and Z-body axes, respectively, slug-ft^2 (kg-m^2)
$\frac{I_X - I_Y}{mb^2}$	inertia yawing-moment parameter
$\frac{I_Y - I_Z}{mb^2}$	inertia rolling-moment parameter
$\frac{I_Z - I_X}{mb^2}$	inertia pitching-moment parameter
m	airplane mass, slugs (kg)
M_Z	yawing moment about Z-body axis, ft-lb (m-N)
r	angular velocity about Z-body axis, rad/sec
S	wing area, ft^2 (m^2)
V	resultant linear velocity, ft/sec (m/sec)
α	angle of attack, deg
β	angle of sideslip, deg
μ_b	airplane relative density, $\frac{m}{\rho Sb}$
ρ	air density, slug/ft^3 (kg/m^3)
ϕ	angle between Y-body axis and horizontal, deg, measured in vertical plane
Ω	resultant angular velocity, rad/sec
$\frac{\Omega b}{2V}$	nondimensional spin-rate coefficient

$$C_{n_r} = \frac{\partial C_n}{\partial \frac{rb}{2V}}$$

$$C_{n_{\dot{\beta}}} = \frac{\partial C_n}{\partial \frac{\dot{\beta} b}{2V}}$$

A dot over a symbol represents differentiation with respect to time; for example, $\dot{\beta} = \frac{d\beta}{dt}$.

DESCRIPTION OF AIRPLANE AND SPIN-RECOVERY TECHNIQUE

The airplane studied in the investigation is shown in figure 1. Some of the more important dimensional characteristics of the airplane are listed in table I, and the mass characteristics are given in table II. The longitudinal control system of the airplane includes an all-movable horizontal tail (stabilator) which incorporates 23° negative geometric dihedral (droop) to satisfy requirements of longitudinal stability in the normal operational flight range. The airplane lateral control system includes upper-surface spoilers as well as ailerons. The ailerons deflect downward while the spoilers deflect upward. The left aileron and right spoiler operate simultaneously as do the right aileron and left spoiler. The directional control system consists of a conventional rudder. The normal maximum control-surface deflections (measured perpendicular to the control-surface hinge lines) are as follows:

Rudder deflection, deg	30 right, 30 left
Stabilator deflection (trailing edge), deg	21 up, 9 down
Aileron deflection, deg	0 up, 30 down
Spoiler deflection, deg	45 up, 0 down

Typical loading conditions result in most of the mass being distributed along the fuselage; consequently the values of I_Z and I_Y are about five times as great as those of I_X. As pointed out in reference 1, the most effective way to obtain antispin yawing moments for recovery of configurations having low values of I_X may be to roll the airplane about the axis of least inertia (in this case, about the X-body axis) in such a direction that a gyroscopic antispin moment is produced. This technique has been verified by past experience with a large number of airplane configurations including the present configuration. Hence, the recommended control recovery technique for the present configuration is simultaneous movement of the ailerons to full with the spin (stick right for a right spin), full aft stick, and rudder full against the direction of rotation; when the yaw rate stops, the stick should be moved to neutral and the rudder and ailerons neutralized to prevent possible spin reversals.

METHOD OF APPROACH

Initially, it was believed that study of the flat spin by use of digital-computer techniques might be an effective means of analyzing factors affecting the flat spin. Accordingly, a series of wind-tunnel tests was undertaken to supply aerodynamic input data for the computer program. The initial tests consisted of static and dynamic (forced-oscillation) tests over a wide range of angle of attack and angle of sideslip. Examination of the results of the initial tests produced a lead as to the cause of the flat spin and, subsequently, additional tests including rotary-balance tests, smoke and tuft-flow visualization tests, single-degree-of-freedom autorotational tests, and free-spinning tests were conducted to determine definitely the cause of the flat spin and to indicate possible modifications to the airplane to effect recovery.

Static and Forced-Oscillation Tests

Static and forced-oscillation tests were conducted with a 1/11-scale model to obtain aerodynamic characteristics of the vehicle over a large range of angle of attack and angle of sideslip at low subsonic speeds. The tests were conducted at the Langley Research Center in a low-speed wind tunnel with a 12-foot (3.66-m) octagonal test section at a Reynolds number of 0.54×10^6 based on the mean aerodynamic chord of the wing. Measurements were made of the static force and moment components over an angle-of-attack range of 0° to 90° for a range of sideslip angles of $\pm 40^\circ$. The forced-oscillation tests were conducted over an angle-of-attack range of 0° to 90° by using the small-amplitude forced-oscillation technique described in detail in reference 2. These tests were made for oscillation amplitudes of $\pm 5^\circ$ and $\pm 10^\circ$ for frequencies of 1.0 and 0.7 cycles per second. Unpublished static-force test data measured at the Ames Research Center on a 1/15-scale model at high Reynolds number were also used in the analysis.

Rotary-Balance Tests

Six-component measurements of forces and moments during spinning motions were made by using the rotary-balance test technique described in detail in reference 3. An internal six-component strain-gage balance was used to measure data as the model was forced to rotate about a spin axis by a motor-driven sting. Rotary-balance measurements were made for an angle-of-attack range of 30° to 90° for a range of sideslip angles of $\pm 15^\circ$. The tests were conducted with the 1/11-scale model in the Langley spin tunnel at a Reynolds number of 0.36×10^6 based on $\bar{c}$.

Autorotation Tests

Single-degree-of-freedom autorotation tests were conducted in the 12-foot (3.66-m) tunnel with the test setup shown in figure 2. The 1/11-scale model was spindle-mounted

at 90° angle of attack on a freely rotating sting such that a single degree of freedom in yaw with 360° turn capability was provided. Autorotative tendencies of the complete configuration with 0° bank (resulting in a sideslip angle of 0°) were investigated as well as autorotative characteristics of the main airframe components. No measurements of aerodynamic forces or moments were made during the autorotation tests.

Flow Visualization Tests

Flow visualization tests were also made in an effort to define more fully the phenomenon causing autorotative tendencies. These tests consisted of tuft studies during the autorotation tests and smoke studies under static conditions at various sideslip angles.

Spin-Tunnel Tests

Tests with a 1/30-scale model were conducted in the Langley spin tunnel to determine the effects of configuration modifications suggested by the results of the foregoing tests. For these tests a 1/30-scale spin model was launched in a flat spin with prerotation into the vertically rising windstream. Mass characteristics of the model are given in table II. The tests provided information regarding (1) modifications necessary to insure recovery from the developed flat spin and (2) modifications necessary to eliminate the flat spin entirely for the configuration.

RESULTS AND DISCUSSION

The present paper presents a general discussion of all pertinent tests performed in the investigation but presents only samples of the detailed data as needed to support the analysis. The results of the tests indicate that the flat-spin autorotational tendencies of the airplane are caused by aerodynamic autorotational moments which result from aerodynamic interference between the horizontal and vertical tail surfaces. The following discussion presents a description of the steps taken and the rationalization used in the investigation.

Forced-Oscillation Tests

The most significant result of the static and dynamic force tests with relation to the flat spin was the indication of propelling or autorotational yawing moments due to rate of rotation for the range of angle of attack associated with the flat spin. Presented in figure 3 is the variation of the damping-in-yaw parameter $C_{n_r} - C_{n_{\dot{\beta}}} \cos \alpha$ with angle of attack as measured during forced-oscillation tests in yaw. Negative values of $C_{n_r} - C_{n_{\dot{\beta}}} \cos \alpha$ are stabilizing (damping), whereas positive values are destabilizing (autorotational). As can be seen, positive values of $C_{n_r} - C_{n_{\dot{\beta}}} \cos \alpha$ existed for the high angles of attack (about 73° to 90°) associated with the flat spin. The values of the

propelling moments were quite large; for example, the magnitude of the propelling moment due to rate of rotation at 90° angle of attack was about equal to the stabilizing values of damping in yaw at 0° angle of attack. The significance of the positive values of $C_{n_r} - C_{n_{\dot{\beta}}} \cos \alpha$ in the angle-of-attack range from 34° to 46° is not obvious at the present time and has not been analyzed.

The aerodynamic data measured during the static and forced-oscillation tests were used in a digital-computer program which used nonlinear, six-degree-of-freedom equations of motion in an attempt to calculate the developed flat spin exhibited by the airplane. As might be expected, the propelling values of $C_{n_r} - C_{n_{\dot{\beta}}} \cos \alpha$ shown in figure 3 led to spins of ever-increasing spin rate. Because this result was not the same as that of flight and previous spin-tunnel tests, which showed a steady flat spin, it was concluded that the aerodynamic damping in yaw of the airplane at extremely high angles of attack was nonlinear with respect to rate of rotation. Similar nonlinear trends of damping in yaw at high angles of attack have also been noted in other spin studies (refs. 1 and 4).

Rotary-Balance Tests

The results obtained from the rotary-balance tests confirmed the nonlinear variation of yawing moment with rate of rotation. For example, shown in figure 4 is the variation of yawing-moment coefficient C_n with nondimensional rate of rotation $\frac{\Omega b}{2V}$ for an angle of attack of 85° during a flat spin to the left. Negative values of C_n correspond to nose-left yawing moments which for the left spin are propelling or autorotative moments. The data of figure 4 show that at low spin rates, such as those used during the forced-oscillation tests $\left(\frac{\Omega b}{2V} = 0.015\right)$, propelling moments are produced by the rate of spin, whereas at higher rates of rotation the propelling moments become smaller and approach zero and thereby lead to a potential stabilized autorotation or steady-spin condition. The equilibrium rate of rotation at 85° angle of attack is indicated by these data as being about 0.24.

In order to identify the airframe components producing the propelling moments, the relationship of the yawing moment and side force acting on the airplane during a spin must be analyzed. Figure 5 shows a top view of the airplane during a flat spin to the left. If the fuselage nose is assumed to produce the propelling moments, a side force to the left, which produces a nose-left (propelling) yawing moment will exist. However, if the tail components are propelling the airplane, the nose-left yawing moments will be produced by a side force to the right. The force-test data obtained for the present configuration indicated that the tail components of the airplane were responsible for the flat-spin tendencies.

After the rear of the airplane was identified as the source of the autorotative tendencies, additional rotary-balance tests were conducted to identify the particular component responsible for the propelling moments. The results of the tests are presented in figure 6

which shows the variation of C_n with nondimensional rate of rotation $\frac{\Omega b}{2V}$ for several tail configurations. When the horizontal tail was removed from the complete configuration, the data indicate that positive (nose-right) yawing moments which tended to oppose the yaw rate were produced. This result is opposite to that for the basic configuration. When the vertical tail was removed, with the horizontal tail on, the resulting configuration showed $C_n = 0$ with little variation for values of $\frac{\Omega b}{2V}$ up to about 0.2. This result indicates a condition of zero or neutral damping in yaw. Data showing the effects of inverting the horizontal tail so that it had positive dihedral are presented. These data show a marked improvement over the damping-in-yaw characteristics of the basic configuration. These results indicate the existence of an interference effect between the vertical and horizontal tail surfaces such that propelling moments are produced only when vertical and horizontal tail surfaces are in position on the airplane.

Static-Force Tests

The forced-oscillation and rotary-balance tests therefore indicated the aerodynamic phenomenon and airframe components responsible for the flat spin. It was highly desirable, however, to be able to analyze the spin problem in terms of conventional static wind-tunnel data which are easier to obtain and can readily be used to analyze the effects of such variables as Reynolds number. In order to interpret the results of static-force tests in terms of the effect of tail configuration on the flat spin, the flow conditions at the tail location during a spin must be known.

The sideslip angle generated at the tail during a flat spin to the left is illustrated in figure 7. The arrows along the fuselage indicate the relative magnitude and sense of the linear sideward velocities imparted along the fuselage by the rate of rotation during a left spin. The sketch at the right of figure 7 is a cross section of the tail during a spin. As can be seen, the airplane rate of descent and the sideward velocity at the tail location produced by the rate of rotation combine vectorially to produce a positive sideslip angle at the tail. With this concept in mind, the variation of static yawing moment with sideslip angle can be examined and the data can be interpreted in a dynamic sense. For example, presented in figure 8 is the variation of static yawing moment with angle of sideslip for the basic configuration at 85° angle of attack. Results are shown for the low Reynolds number tests conducted at the Langley Research Center and for tests at a considerably higher value of Reynolds number conducted at the Ames Research Center. The data show that the basic configuration produced negative (nose-left) yawing moments when subjected to sideslip angles from 0° to approximately 20° or 25°. From the preceding analysis, the nose-left yawing moments may be interpreted as propelling moments for a left spin. The results also indicate a decrease in the magnitude of the prospin moment as Reynolds number was increased from 0.54×10^6 to 5.40×10^6, but the basic trend of prospin moments with sideslip angle is seen to be the same for the two values of Reynolds

number. It should be noted that the static-force test data exhibit a nonlinear variation with sideslip angle similar to that of the rotary-balance data of figure 4.

The results of additional static-force tests illustrating the effect of various tail configurations on the variation of static yawing-moment coefficient with sideslip angle are shown in figure 9. The data of figure 9(a) indicate trends similar to those exhibited by the rotary-balance data of figure 6; that is, removal of either the vertical or horizontal tail or inversion of the horizontal tail so that it had positive dihedral produced nose-right or damping moments over the entire range of positive sideslip angles.

At this stage of the study, it seemed that the aerodynamic interference effects produced by the tail configuration of the airplane may have been caused by either geometric dihedral or by the fact that the negative dihedral effectively changed the vertical location of the tips of the horizontal tail. A series of tests with a horizontal tail having 0° dihedral at several vertical locations was therefore conducted to determine the influence of vertical location of the horizontal tail. The results of these tests are presented in figure 9(b). When the negative dihedral was removed from the basic horizontal tail, the propelling moments were eliminated. Lowering the horizontal tail with 0° dihedral however produced propelling moments similar to the basic configuration with negative dihedral. These data indicate that the main effect of the negative dihedral of the horizontal tail was a lowering of the horizontal tail area into a vertical position which was conducive to aerodynamic interference between the horizontal tail and the vertical tail.

Inasmuch as tail geometry was found to have a significant effect on the propelling tendencies, additional static-force tests were conducted to investigate the effects of horizontal tail incidence angle on yawing moment; the results of these tests are presented in figure 10. These data show the variation of yawing moment with sideslip angle for horizontal tail incidence angles of 21°, 40°, and 55°, trailing edge up, and data are also presented for the horizontal tails removed. The present physical deflection limit on the airplane is 21°, and the test results indicate that the propelling tendencies are still present. Increasing the deflection angle to 55° however appears to be about as effective in eliminating the propelling moment as removing the horizontal tails altogether.

Autorotation Tests

The steady nonoscillatory nature of the flat spin exhibited by the airplane and the fact that the configuration spun about an axis passing approximately through the center of gravity led to the belief that single-degree-of-freedom autorotational tests could be used to investigate the flat spin in the wind tunnel. Autorotation tests should also verify the damping or propelling tendencies resulting from the various tail deflection angles as deduced from the static-force test results of figure 10.

The results of the autorotation tests showed that the basic configuration with controls neutral would (when disturbed) autorotate at 90° angle of attack at the same angular rate in either spin direction. The nondimensional rate of rotation $\frac{\Omega b}{2V}$ was approximately equal to 0.2 and was independent of airspeed. When disturbed from rest, the model would accelerate to this rate of rotation and stabilize; when the model was prerotated to a spin rate faster than $\frac{\Omega b}{2V} = 0.2$, the spin rate would slow down to the autorotational value. The fact that no correction was applied to the nondimensional rate of rotation to account for bearing support friction probably explains why the value of $\frac{\Omega b}{2V}$ was slightly less than that indicated by the rotary-balance data of figure 4. The results of the autorotation tests also showed that the basic configuration would not autorotate when the vertical and horizontal tails were removed simultaneously, as was expected. Also removal of the wing (producing a fuselage-alone configuration) did not result in autorotation.

Additional tests were conducted to determine the effects of tail arrangements on the autorotational tendencies of the complete airplane. The tail configurations studied are indicated in figure 11. When either the vertical or horizontal tail surfaces were removed individually, the propelling moments were eliminated and the model would not autorotate; these results would be expected from the preceding analysis. When the negative dihedral angle of the horizontal tail was increased to 40° or greater, the model would not autorotate. Inversion of the horizontal tail, so that it had positive dihedral, also eliminated autorotation in accordance with the rotary-balance and static-force test results. Relocation of the vertical tail in a more forward position (moved forward a distance equal to $\bar{c}_t$) also produced a stable configuration. When the area vacated by the vertical tail was filled by an auxiliary panel, however, the model again autorotated. Tail incidence angles equal to or greater than 40° in either direction eliminated autorotation, as expected based on the data of figure 10. This modification appears to be the most acceptable for a production airplane. Strakes were investigated on the vertical tail surface and on the rear fuselage, but no strake location could be found which would eliminate the strong autorotative tendencies.

Flow Visualization Tests

Tuft and smoke studies were undertaken to obtain a better understanding of the nature of the flow phenomenon causing the propelling moments. Typical tuft patterns along the vertical tail surface of the basic configuration under autorotative conditions for a right spin are presented in figure 12. The tuft pattern in figure 12(a) illustrates the flow on the advancing side of the vertical tail during a right spin, whereas figure 12(b) shows the flow pattern on the opposite trailing side. The flow pattern on the advancing side indicated the presence of a vortex between the vertical and horizontal tail surfaces. During the autorotation tests, it was observed that, under nonrotating conditions, vortices shed by the separated bluff-body flow past the horizontal tail impinged symmetrically on

either side of the upper part of the vertical tail. (The top row of tufts indicated flow reversal such as shown in fig. 12(a) at the upper part of the vertical tail.) The flow however appeared to be unstable, and one side of the vertical tail or the other would quickly conform to the flow pattern of figure 12(a) and autorotation would begin. During the tests the model would autorotate of its own accord either to the right or to the left; there was no tendency for the model to begin autorotation in one direction more than in the other.

Additional smoke and tuft studies were made under static conditions with the model sideslipped at 90° angle of attack. Typical smoke patterns about the rear end of the model are presented in figure 13. As shown in the photograph and sketch of figure 13(a), flow about the rear end of the model at $\beta = 0^{\circ}$ consisted of separated bluff-body flow with free boundary-layer flow similar to the flow pattern behind inclined flat plates as described in reference 5. The vortex layers were observed to roll up into wake vortices farther downstream, with slight impingement on the upper vertical tail as observed during the autorotation tuft studies. This type of flow also existed around the entire perimeter of the horizontal tail surfaces; the flow separation from the leading and trailing edges of the stabilator is also to be considered as contributing to the flow phenomenon. When the sideslip angle was increased to 10° (as would be the case at the tail for a left spin), as shown in figure 13(b), the vortex layer on the trailing side moved outboard while the vortex layer on the advancing side formed two distinct vortex patterns as depicted in the sketch. This flow pattern conforms to that observed by tufts on the vertical tail surfaces during autorotation (fig. 12). This flow pattern, observed under static conditions, would seem to be the flow pattern at the tail associated with autorotation. The fact that the flow field is observed to be quite large is probably why strakes on the vertical tail were found to be relatively ineffective during the autorotation tests. The flow from the leading and trailing edges of the horizontal tail is believed to be as important to the flow phenomenon as the flow from the tip of the horizontal tail.

Spin-Tunnel Tests

The spin-tunnel test results are shown in charts 1 and 2. In the spin charts control positions are shown for spin entry. Results for elevator up (stick back) are presented at the top of the charts and results for elevator down (stick forward), at the bottom of the charts; results for the ailerons-with-the-spin condition (stick right in the right spin) are presented on the right side of the charts and results for the ailerons-against-the-spin condition (stick left), on the left side of the charts.

Tests in the spin tunnel showed that the classical fast flat spin could be obtained with the horizontal tail either deflected 21° trailing edge up or neutral, and with the ailerons either neutral or against the spin. Spin recovery from the flat spin with the best possible recovery-control technique (deflection of the rudder to full against the spin,

deflection of the ailerons to full with the spin, and deflection of the horizontal tail to 21° trailing edge up) was unsatisfactory.

Tests to check the effects in actual spins of the various recovery techniques and configuration modifications suggested by the results of the tests described in the preceding sections of this paper were directed at the following two objectives:

(1) Evaluation of techniques which might permit recoveries from the developed flat spin

(2) Documentation of the apparent adverse effect of the drooped horizontal tail surfaces on the spin characteristics, and evaluation of modifications which might eliminate the flat-spin mode on this design and future airplane designs

In the first phase of the study a series of tests was conducted on the model for two center-of-gravity positions to evaluate the effectiveness of deflecting the horizontal tail trailing edge up 30°, 40°, and 55° for recovery, and also of deflecting the horizontal tail trailing edge up 21°, 30°, and 40° with simultaneous deployment of a 16-foot (4.88-m) landing drag parachute normally carried by the airplane (with the distance from attachment point to canopy increased to 100 feet (30.48 m)). The results are presented in charts 1 and 2. These test results indicate that increasing the trailing-edge-up deflection of the horizontal tail used in the recommended recovery technique to 30° or 40° failed to produce recovery in some cases. The single-degree-of-freedom autorotation tests indicated that 40° deflection of the horizontal tail would change the flow pattern over the tail surfaces sufficiently to prevent autorotation; but these spin-tunnel test results showed that once the flat spin was developed, 40° deflection was not adequate to overcome the high angular momentum of the spin rapidly enough for satisfactory recoveries. When the horizontal tail deflection was increased to 55°, trailing edge up, a significant improvement was obtained in the recovery characteristics and consistent recoveries from the developed spin were obtained in less than five or six turns. When the horizontal tail deflection was increased to 90°, trailing edge up, there did not seem to be any further improvement in recovery. These results indicate that a 55° delfection of the stabilator removes most or all of the flow interference caused by the horizontal tail and the resulting recoveries are considered to be marginally acceptable when considering the high rate of rotation of the spin.

Further improvements of recovery characteristics were obtained by simultaneous use of the increased horizontal tail deflections with deployment of the landing drag parachute normally carried by the airplane. Recoveries attempted by deploying the parachute with a horizontal tail deflection of 21°, trailing edge up, were unsatisfactory. (See chart 2.) When the horizontal tail was deflected to 30°, trailing edge up, with simultaneous deployment of the drag parachute, the recovery characteristics were improved but were considered marginal. By increasing the horizontal tail deflection to 40°, with

parachute deployment, the recovery characteristics were improved to the extent that recoveries were obtained in two to $4\frac{1}{2}$ turns. Recoveries in two to $4\frac{1}{2}$ turns would normally be considered unsatisfactory. In the present case however the recoveries were obtained from a very flat and fast rotating spin and were positive and consistent. The significance of qualification as to the fast-spin rate is that the altitude loss involved in recovery may not be much greater for such a spin that for a $2\frac{1}{2}$-turn recovery from a steep oscillatory spin for which the descent rate is higher.

The test results with regard to the effects of tail dihedral and the relative positions of the vertical and horizontal tails are not presented in the charts. The tests showed however that when the basic drooped horizontal tail surfaces were moved rearward a distance approximately equal to $\bar{c}_t$, the model did not exhibit a flat-spin mode. Likewise, when the geometric dihedral was removed from the horizontal tail or when the horizontal tail was inverted so that the dihedral angle was positive, the model again displayed no flat-spin tendencies. In both cases, even though the model was launched into a flat spin in the tunnel, the flat-spin motion quickly subsided and the model entered a steep oscillatory spin. These results are considered to be quite significant in that recovery from a steep oscillatory spin is usually satisfactory with the recommended control application, whereas no recovery could be effected from the developed flat spin for the basic configuration. These results are a further indication that the autorotational moments caused by the interference effects brought about by the tail configuration were perhaps the most important factor causing the flat spin.

It is important to consider the application of the results of this investigation to other airplane designs. The tail configuration was found to be the primary factor that caused the flat spin exhibited by the configuration investigated. Caution should be used in applying these results to other airplane configurations however. Flat spins are known to exist on other designs with tail surfaces having zero or even positive dihedral; other designs with negative dihedral do not spin flat. Factors other than tail configuration can also predominantly influence the spin characteristics of a given airplane design and can cause a flat spin to occur.

SUMMARY OF RESULTS

An investigation to determine the significant factors contributing to the flat-spin tendencies of a contemporary twin-jet swept-wing fighter airplane has produced the following results:

1. The flat-spin autorotational characteristics of the airplane were caused by aerodynamic autorotational moments which resulted from aerodynamic interference between the horizontal and vertical tail surfaces.

2. Several modifications to the basic airplane tail arrangement were designed to eliminate the aerodynamic causes of the flat spin and consequently either eliminate or provide recovery from this type of spin. The most feasible modification for retrofit to production airplanes seems to be the use of increased trailing-edge-up deflection of the horizontal tail.

3. Marginally acceptable recovery characteristics from the fast flat spin were obtained by use of increased horizontal tail deflection (from 21° to 55°) with deflection of the rudder to against the spin and the ailerons to with the spin.

4. Acceptable recovery characteristics from the fast flat spin were accomplished by deflecting the rudder to full against the spin, the ailerons to full with the spin, the horizontal tail to 40° trailing edge up, and simultaneous deployment of the 16-foot (4.88-m) landing drag parachute with a distance from the attachment point to the canopy equal to 100 feet (30.48 m).

Langley Research Center,
National Aeronautics and Space Administration,
Langley Station, Hampton, Va., July 7, 1969.

REFERENCES

1. Neihouse, Anshal I.; Klinar, Walter J.; and Scher, Stanley H.: Status of Spin Research for Recent Airplane Designs. NASA TR R-57, 1960. (Supersedes NACA RM L57F12.)

2. Hewes, Donald E.: Low-Subsonic Measurements of the Static and Oscillatory Lateral Stability Derivatives of a Sweptback-Wing Airplane Configuration at Angles of Attack from -10° to 90°. NASA MEMO 5-20-59L, 1959.

3. Stone, Ralph W., Jr.; Burk, Sanger M., Jr.; and Bihrle, William, Jr.: The Aerodynamic Forces and Moments on a 1/10-Scale Model of a Fighter Airplane in Spinning Attitudes As Measured on a Rotary Balance in the Langley 20-Foot Free-Spinning Tunnel. NACA TN 2181, 1950.

4. Scherer, Michel; and Louis, Bernard: Étude Analytique de la Vrille. O.N.E.R.A., T.P. No. 187, 1964.

5. Abernathy, F. H.: Flow Over an Inclined Plate. J. Basic Eng., vol. 84, no. 3, Sept. 1962, pp. 380-388.

TABLE I.- DIMENSIONAL CHARACTERISTICS OF AIRPLANE

Overall length	57.59 ft (17.55 m)
Wing:	
Span	38.41 ft (11.71 m)
Area (including leading-edge extension)	538.34 ft^2 (50.01 m^2)
Root chord	282.00 in. (716.28 cm)
Tip chord	47.00 in. (119.38 cm)
Mean aerodynamic chord, $\bar{c}$	192.50 in. (488.95 cm)
Leading edge of $\bar{c}$ rearward of leading edge of root chord	110.76 in. (281.33 cm)
Aspect ratio	2.82
Taper ratio	0.167
Sweepback of 25-percent chord	45.00°
Dihedral (inboard 69.5 percent b/2)	0°
Dihedral (outboard 69.5 percent b/2)	12.00°
Incidence	1.00°
Airfoil section:	
Root	NACA 0006.4-64 (modified)
Tip	NACA 0003.0-64 (modified)
Aileron:	
Area (one side) rearward of hinge line	13.08 ft^2 (1.22 m^2)
Span (one aileron) (from 44.5 to 67.0 percent b/2)	4.35 ft (1.33 m) (22.5 percent b/2)
Inboard end chord (base line 103.24 in. (262.23 cm))	37.81 in. (96.04 cm) (21.3 percent $\bar{c}$)
Outboard end chord (base line 155.44 in. (394.82 cm))	34.38 in. (87.33 cm) (27.6 percent $\bar{c}$)
Spoilers:	
Area (one side)	13.08 ft^2 (1.22 m^2)
Span (from 45.3 to 67.0 percent b/2)	4.19 ft (1.28 m)
Inboard end chord	1.39 ft (0.42 m)
Outboard end chord	1.04 ft (0.32 m)
Horizontal tail:	
Area (in chord plane)	94.70 ft^2 (8.80 m^2)
Movable area	77.40 ft^2 (7.19 m^2)
Span	17.705 ft (5.40 m)
Aspect ratio	3.30
Taper ratio	0.20
Sweepback of 25-percent chord	35.50°
Dihedral	-23.00°
Root chord (at airplane center line)	107.00 in. (271.78 cm)
Tip chord (theoretical)	21.40 in. (54.36 cm)
Airfoil section:	
Root (airplane center line)	NACA 0003.7-64 (modified)
Tip (theoretical)	NACA 0003.0-64 (modified)
Hinge-line location, percent $\bar{c}_t$	41.00
Vertical tail:	
Area	67.50 ft^2 (6.27 m2)
Span	6.38 ft (1.94 m)
Taper ratio	0.227
Root chord	207.15 in. (526.16 cm)
Tip chord	47.10 in. (119.63 cm)
Sweepback of 25-percent chord	58.30°
Airfoil section:	
Root	NACA 0004.0-64 (modified)
Tip	NACA 0002.5-64 (modified)
Rudder:	
Area (rearward of hinge line)	11.07 ft^2 (1.03 m^2)
Hinge-line location, percent of water-line chords	80.00

TABLE II.- MASS CHARACTERISTICS AND INERTIA PARAMETERS USED FOR 1/30-SCALE-MODEL SPIN TESTS

[Values given are full-scale, and moments of inertia are given about center of gravity]

Weight	36 328 lbf (161 594 N)
Center-of-gravity location:	
Vertical	0.042
Horizontal	0.339, 0.304
Relative density, μ_b:	
Sea level	23.22
25 000 ft (7620 m)	51.80
Moments of inertia:	
I_X	26 108 slug-ft^2 (35 397 kg-m^2)
I_Y	116 222 slug-ft^2 (157 574 kg-m^2)
I_Z	131 625 slug-ft^2 (178 457 kg-m^2)
Mass parameters:	
$\frac{I_X - I_Y}{mb^2}$	-599×10^{-4}
$\frac{I_Y - I_Z}{mb^2}$	-93×10^{-4}
$\frac{I_Z - I_X}{mb^2}$	636×10^{-4}

CHART 1.- SPIN AND RECOVERY CHARACTERISTICS OF THE MODEL
FOR CENTER-OF-GRAVITY POSITION OF 30.4% $\bar{c}$

[Recovery attempted as noted (recovery attempted from, and developed spin data presented for rudder-full-with spins)]

Airplane	Attitude	Direction	Loading
	Erect	Right	See table II
Stats	Flaps		Center-of-gravity position: 30.4% $\bar{c}$
			Altitude: 25 000 ft (7 620 m)

Model values converted to full scale

U - inner wing up D - inner wing down

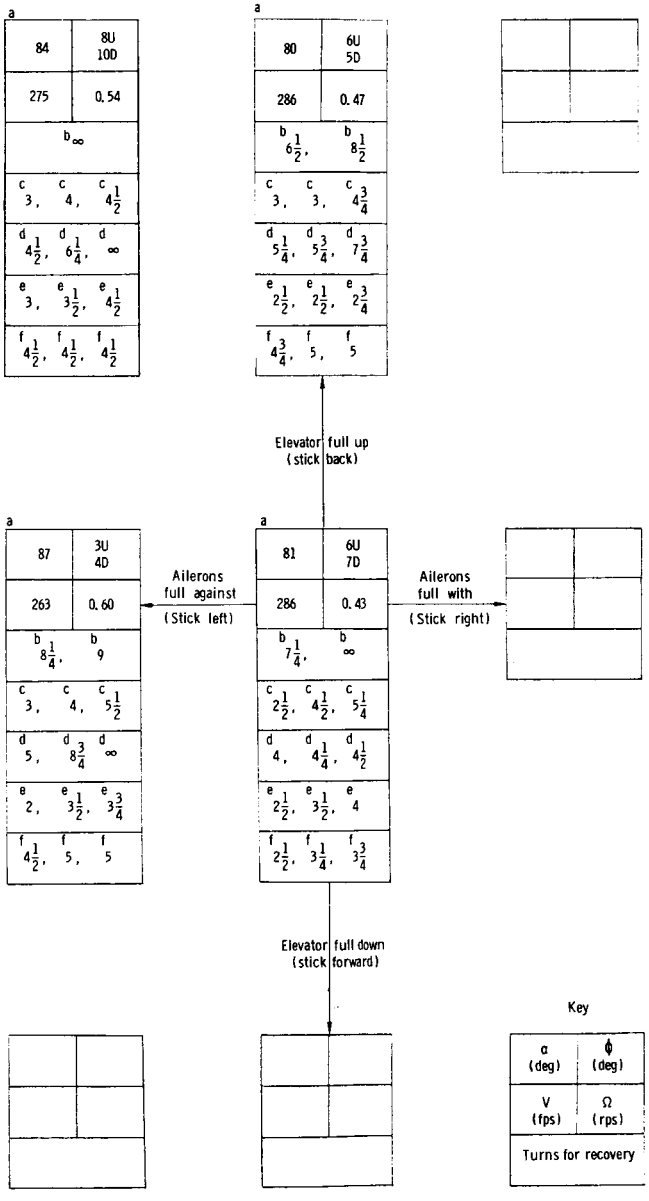

[a]Fast, flat spin.

[b]Recovery attempted by moving rudder to 30° against the spin, ailerons to 30° with the spin, and elevator to 30° up.

[c]Recovery attempted by moving rudder to 30° against the spin, ailerons to 30° with the spin, elevator to 30° up, and deploying landing drag parachute.

[d]Recovery attempted by moving rudder to 30° against the spin, ailerons to 30° with the spin, and elevator to 40° up.

[e]Recovery attempted by moving rudder to 30° against the spin, ailerons to 30° with the spin, elevator to 40° up, and deploying landing drag parachute.

[f]Recovery attempted by moving rudder to 30° against the spin, ailerons to 30° with the spin, and elevator to 55° up.

CHART 2.- SPIN AND RECOVERY CHARACTERISTICS OF THE MODEL FOR CENTER-OF-GRAVITY POSITION OF 33.9% $\bar{c}$

[Recovery attempted as noted (recovery attempted from, and developed spin data presented for rudder-full-with spins)]

Airplane	Attitude	Direction	Loading
	Erect	Right	See table II
Slats	Flaps		Center-of-gravity position: 33.9% $\bar{c}$ / Altitude: 25 000 ft (7 620 m)

Model values converted to full scale

U - inner wing up D - inner wing down

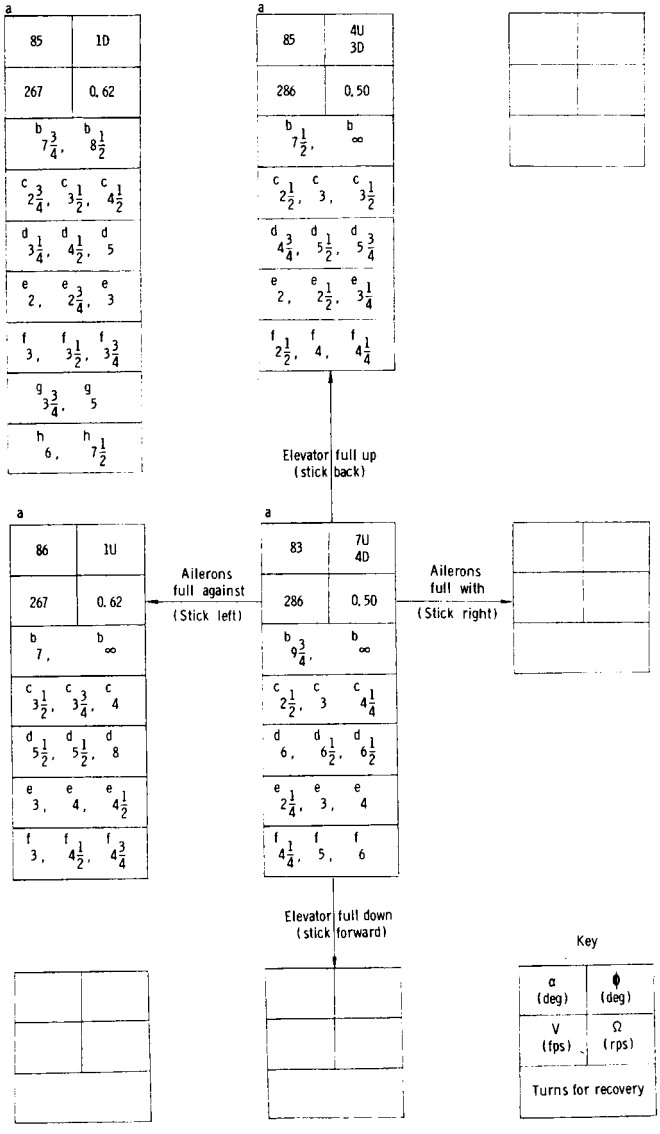

[a]Fast, flat spin.

[b]Recovery attempted by moving rudder to 30° against the spin, ailerons to 30° with the spin, and elevator to 30° up.

[c]Recovery attempted by moving rudder to 30° against the spin, ailerons to 30° with the spin, elevator to 30° up, and deploying landing drag parachute.

[d]Recovery attempted by moving rudder to 30° against the spin, ailerons to 30° with the spin, and elevator to 40° up.

[e]Recovery attempted by moving rudder to 30° against the spin, ailerons to 30° with the spin, elevator to 40° up, and deploying landing drag parachute.

[f]Recovery attempted by moving rudder to 30° against the spin, ailerons to 30° with the spin, and elevator to 55° up.

[g]Recovery attempted by moving rudder to 30° against the spin and the elevator to 90° up.

[h]Recovery attempted by deploying only the landing drag parachute.

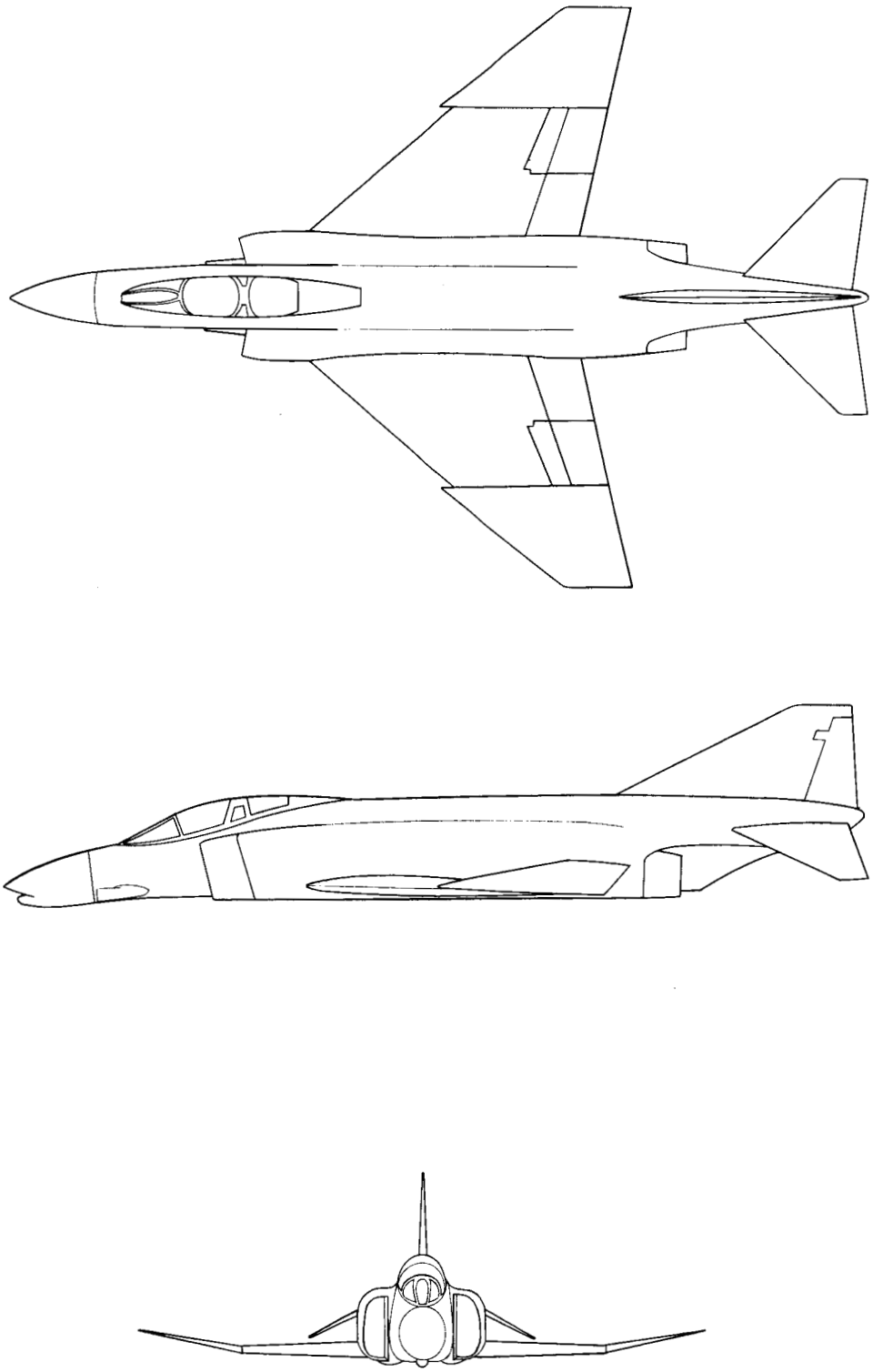

Figure 1.- Three-view sketch of airplane configuration.

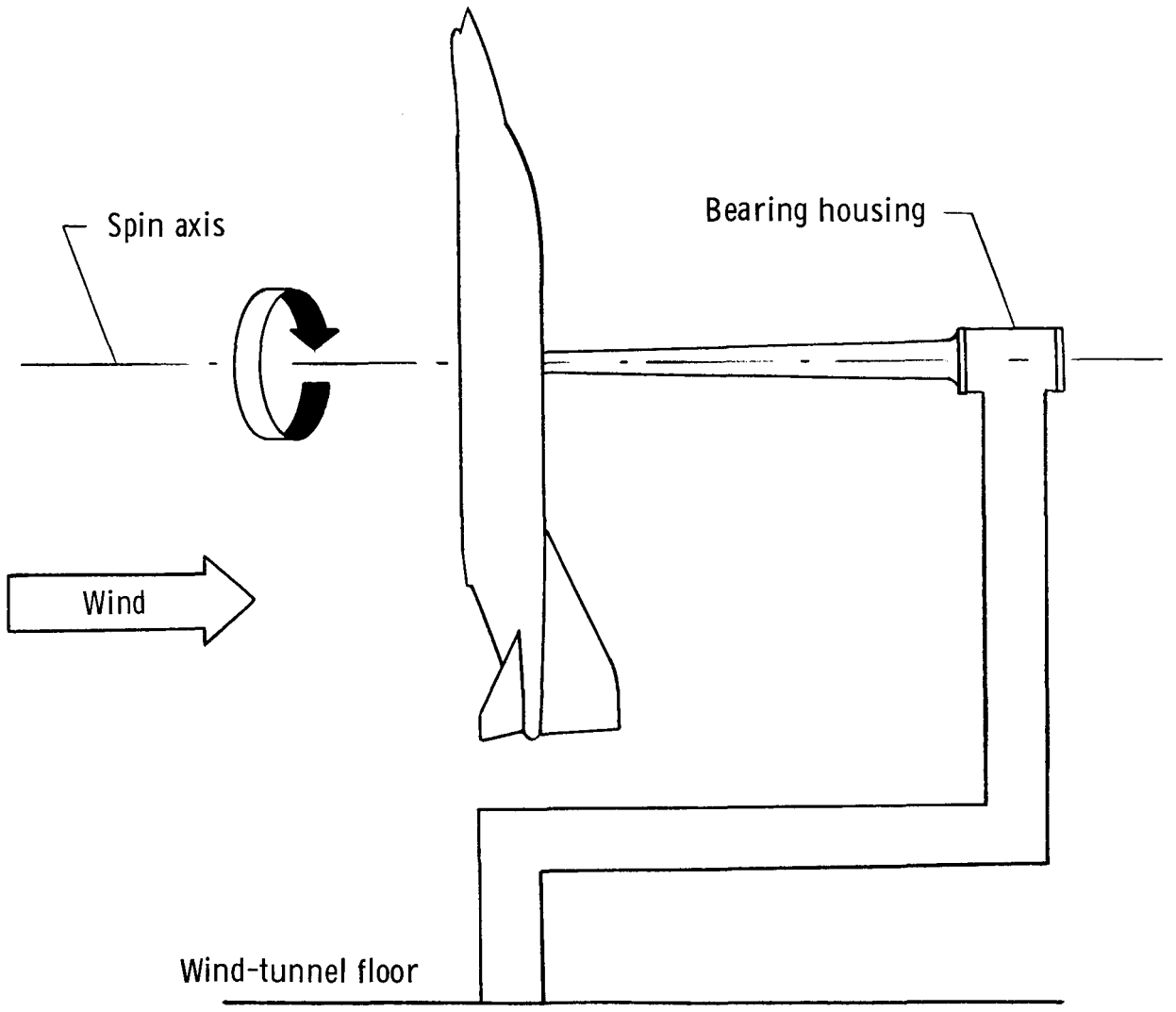

Figure 2.- Sketch of test setup for single-degree-of-freedom autorotation tests.

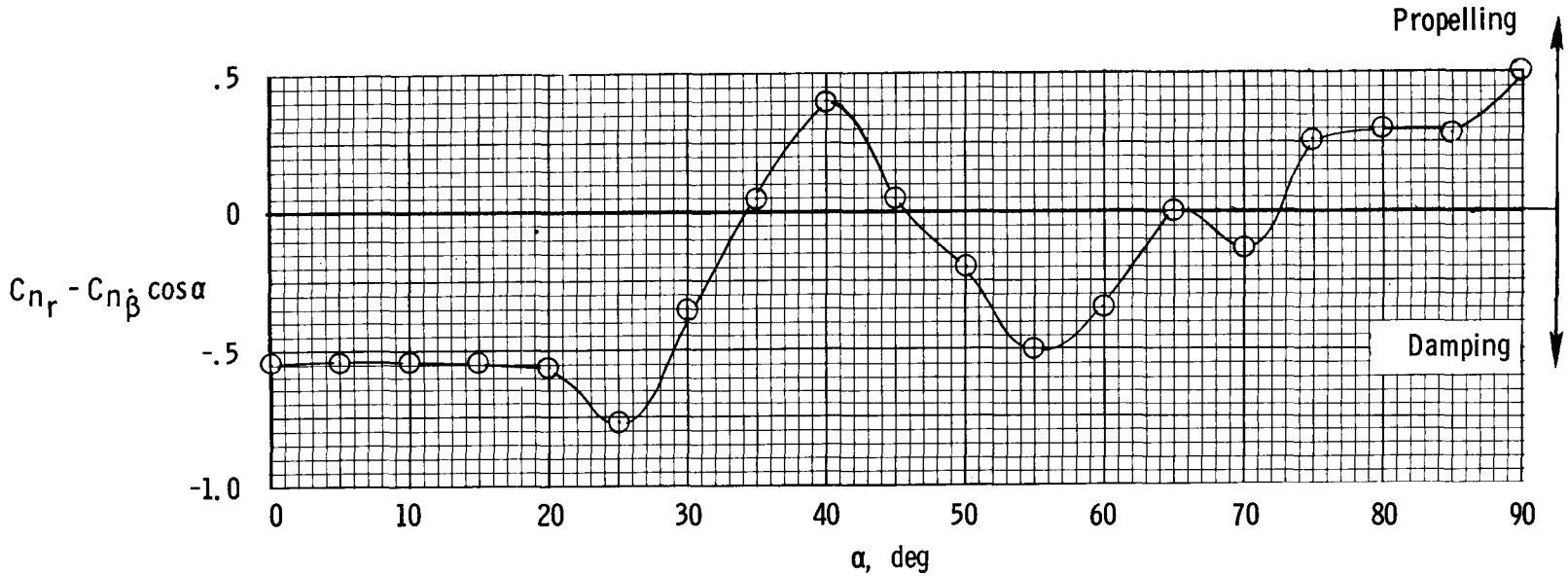

Figure 3.- Variation of aerodynamic damping-in-yaw parameter with angle of attack. $\frac{\Omega b}{2V} = 0.015$; $i_t = 0^o$.

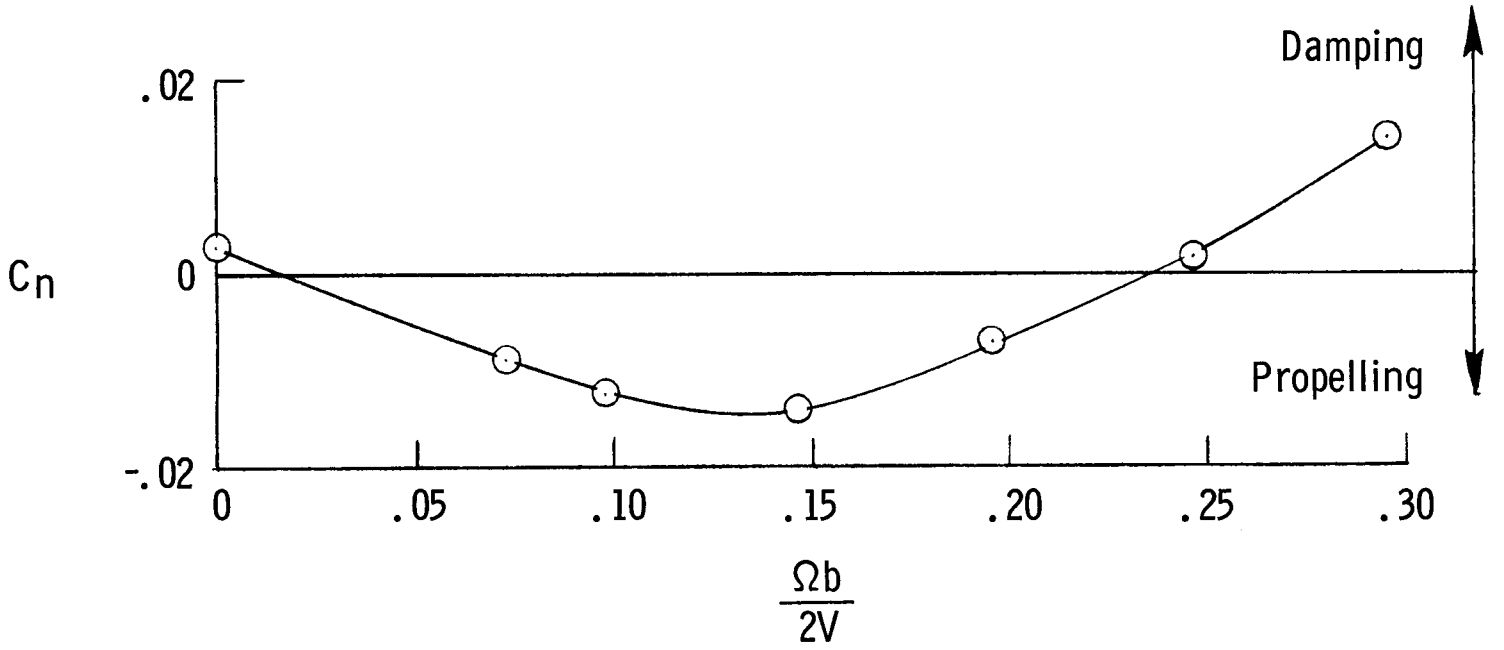

Figure 4.- Variation of yawing moment with rate of rotation. Left spin; $\alpha = 85^0$; $i_t = 0^0$.

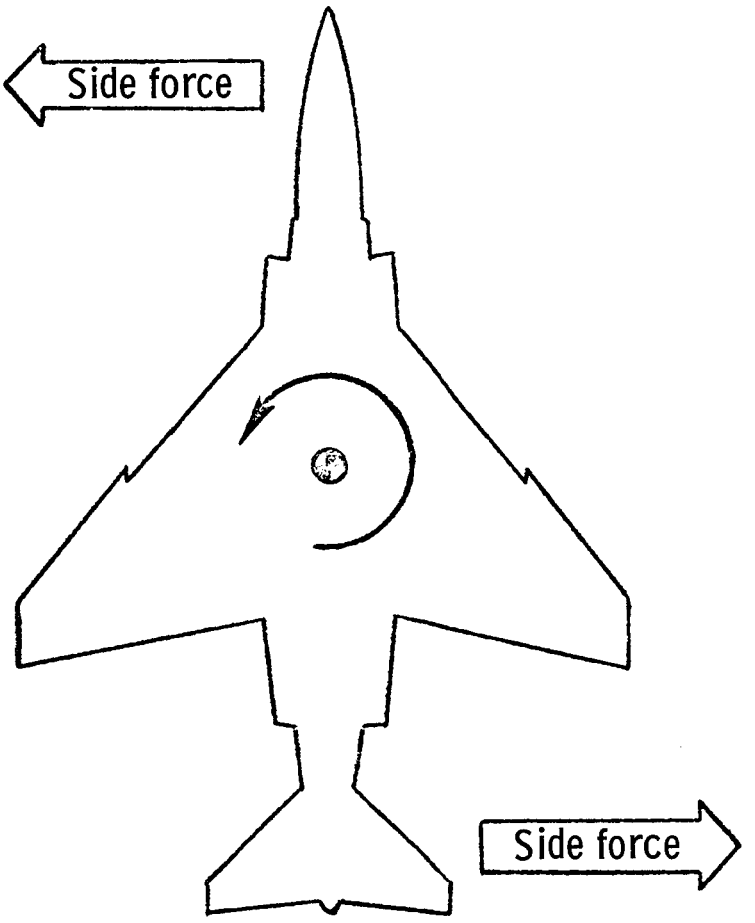

Figure 5.- Assumed relationship between side force and yawing moment during flat spin to left.

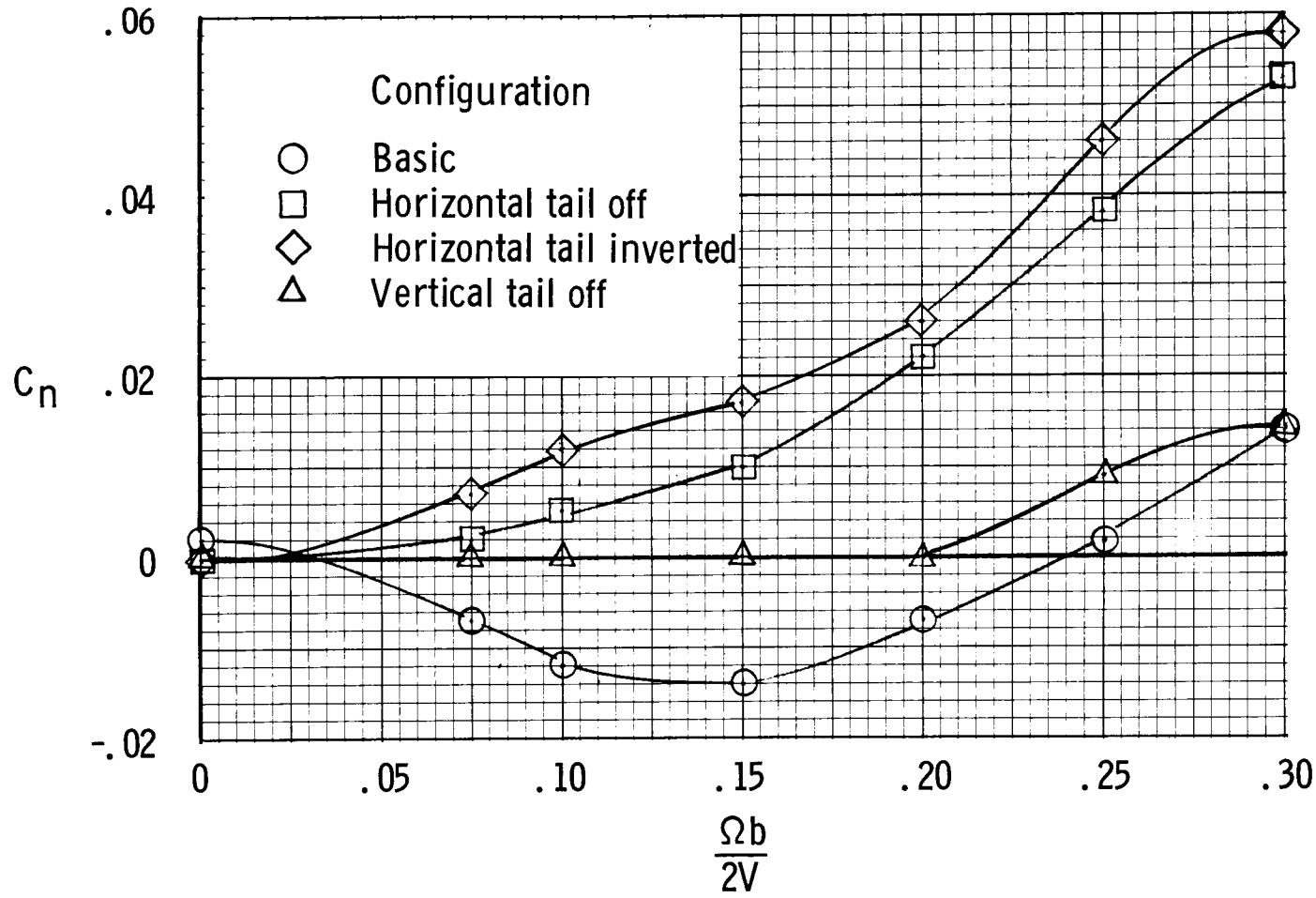

Figure 6.- Variation of yawing-moment coefficient with nondimensional rate of rotation for several tail configurations. $\alpha = 85^0$; left spin; $i_t = 0^0$.

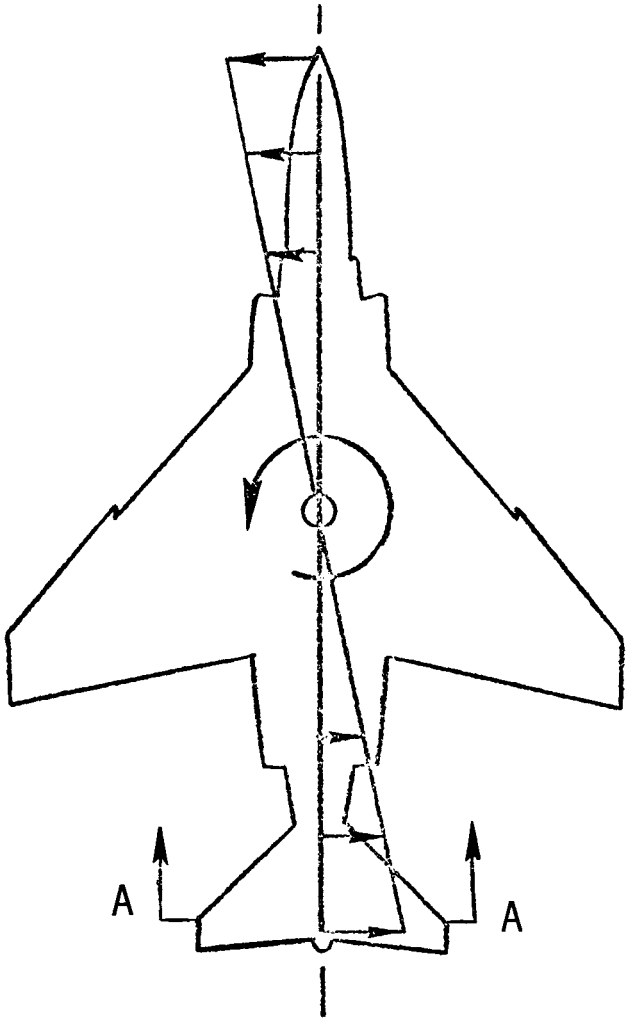

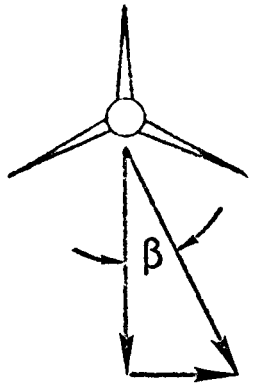

Section
A - A

Figure 7.- Sideslip angle generated at tail during flat spin to left.

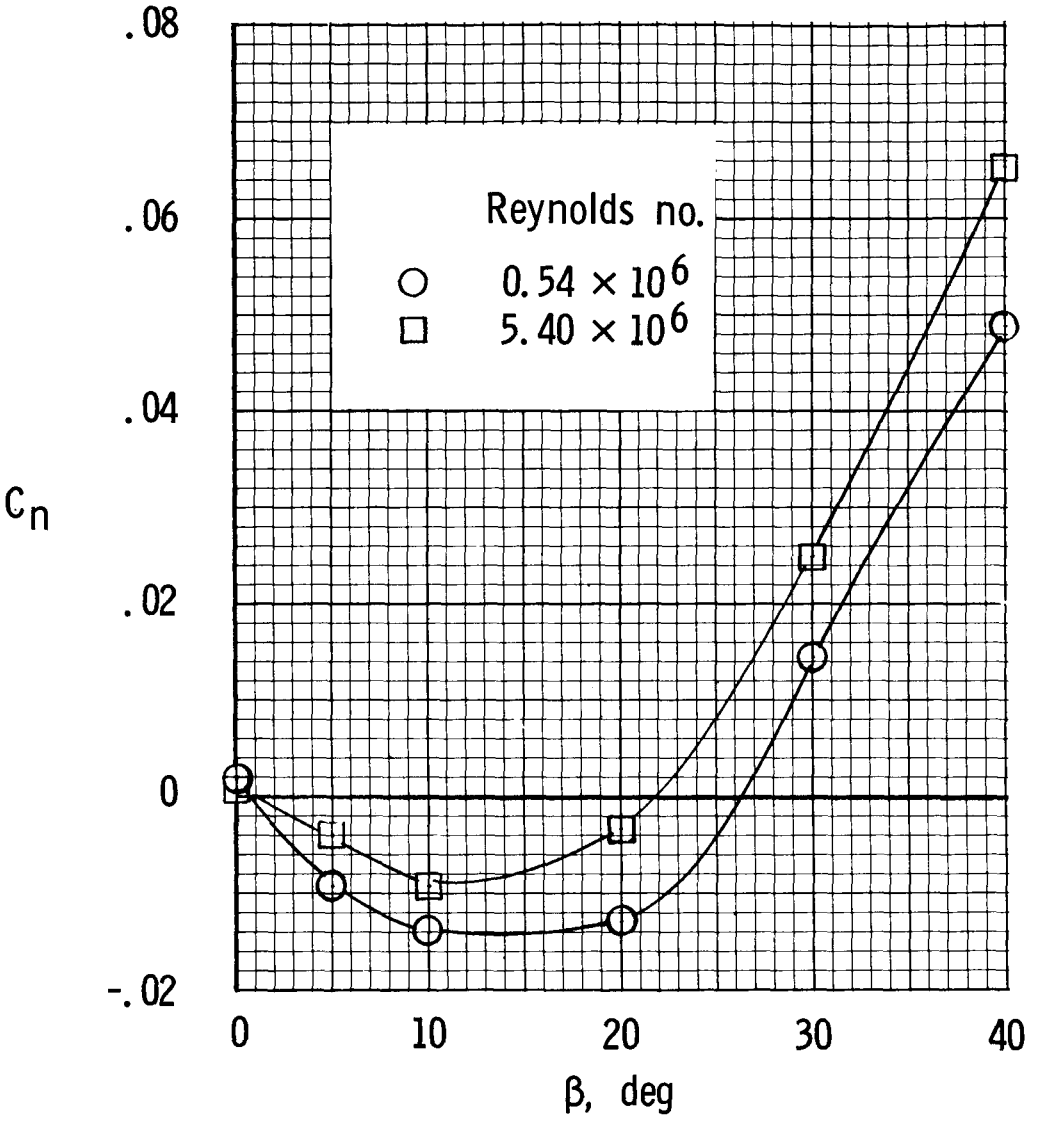

Figure 8.- Effect of Reynolds number on static yawing-moment coefficient for basic configuration. $\alpha = 85^0$; $i_t = 0^0$.

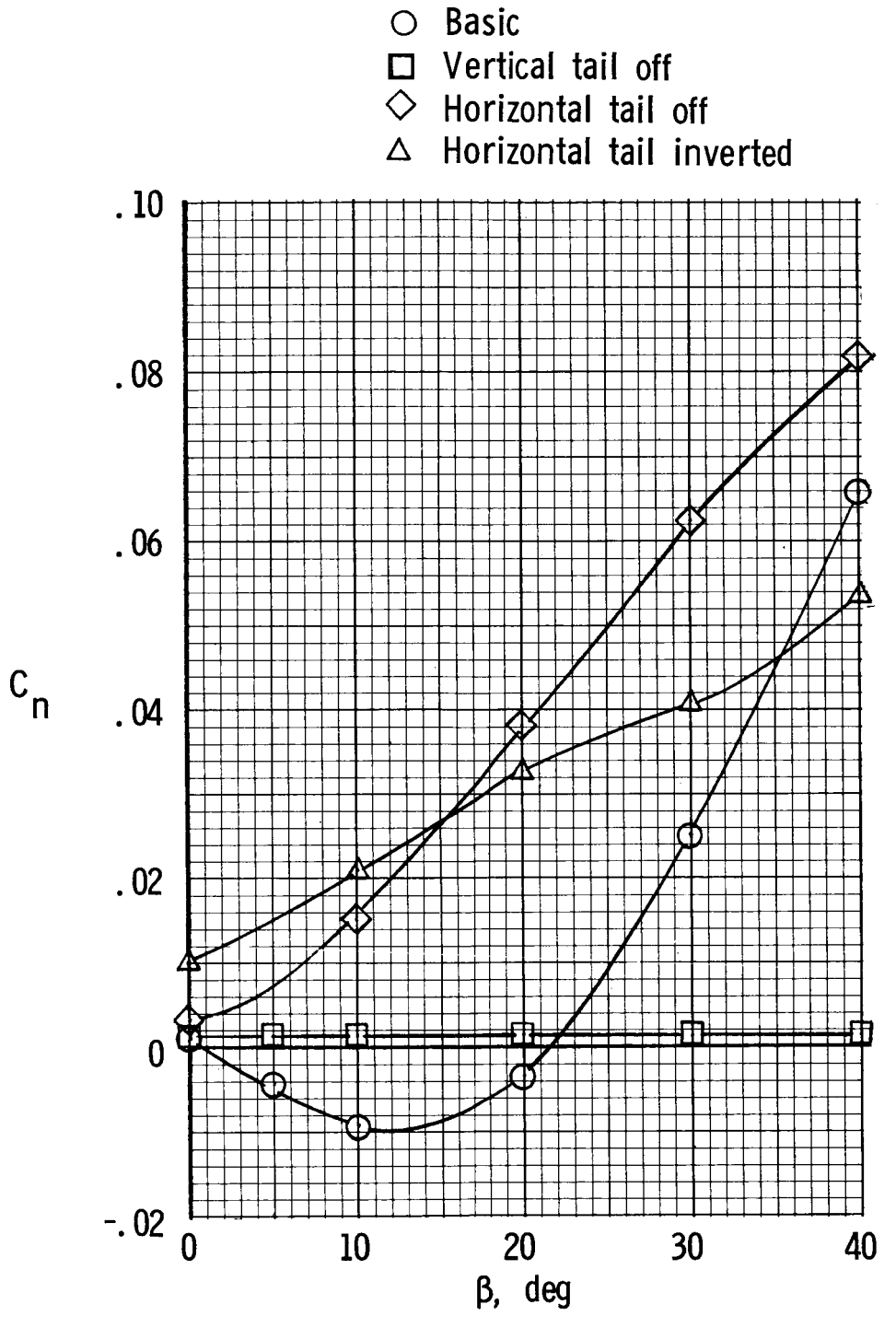

(a) Effect of individual components.

Figure 9.- Variation of static yawing-moment coefficient with sideslip angle for several tail configurations. $\alpha = 85^0$; $i_t = 0^0$.

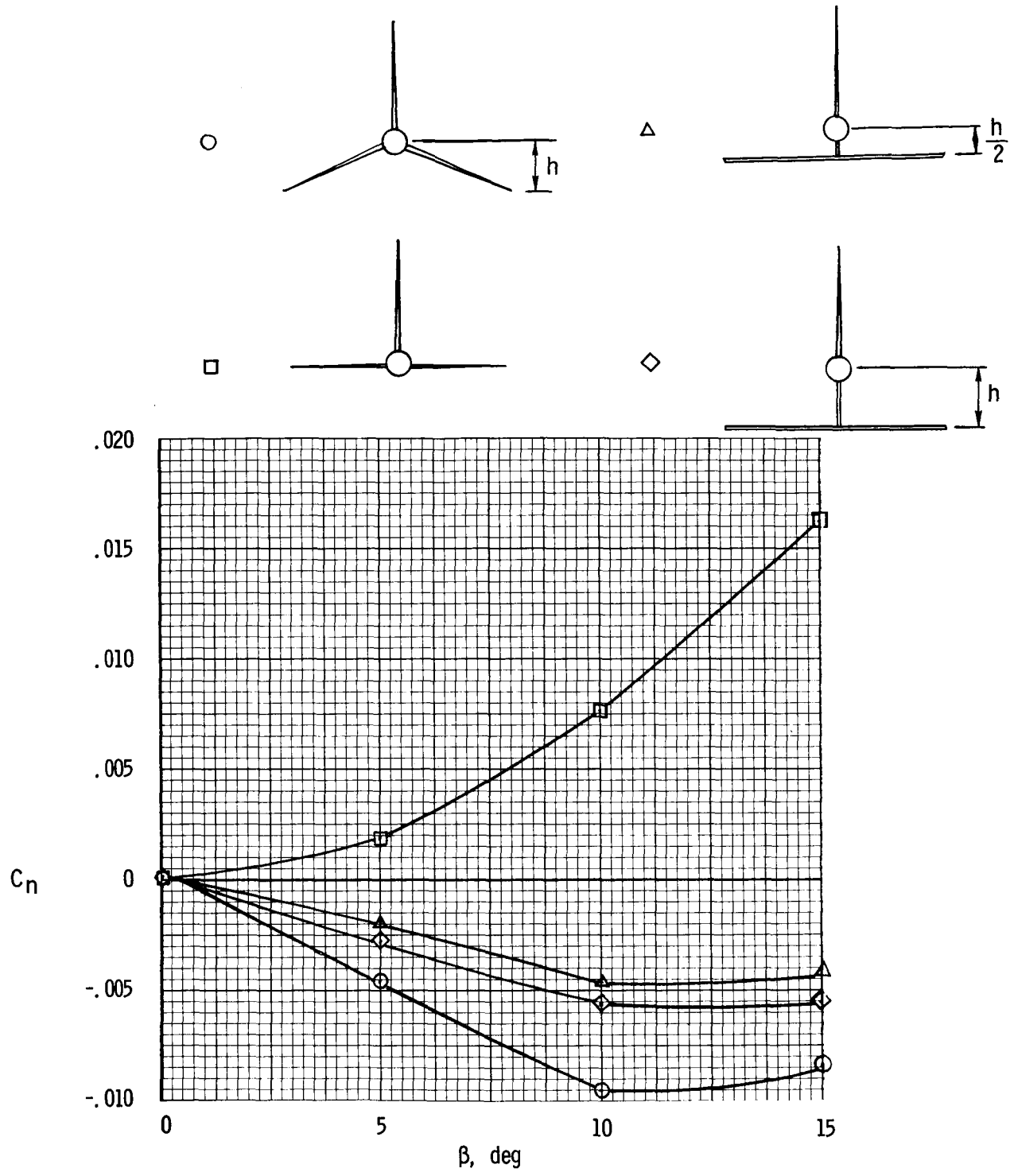

(b) Effect of vertical location of horizontal tail.

Figure 9.- Concluded.

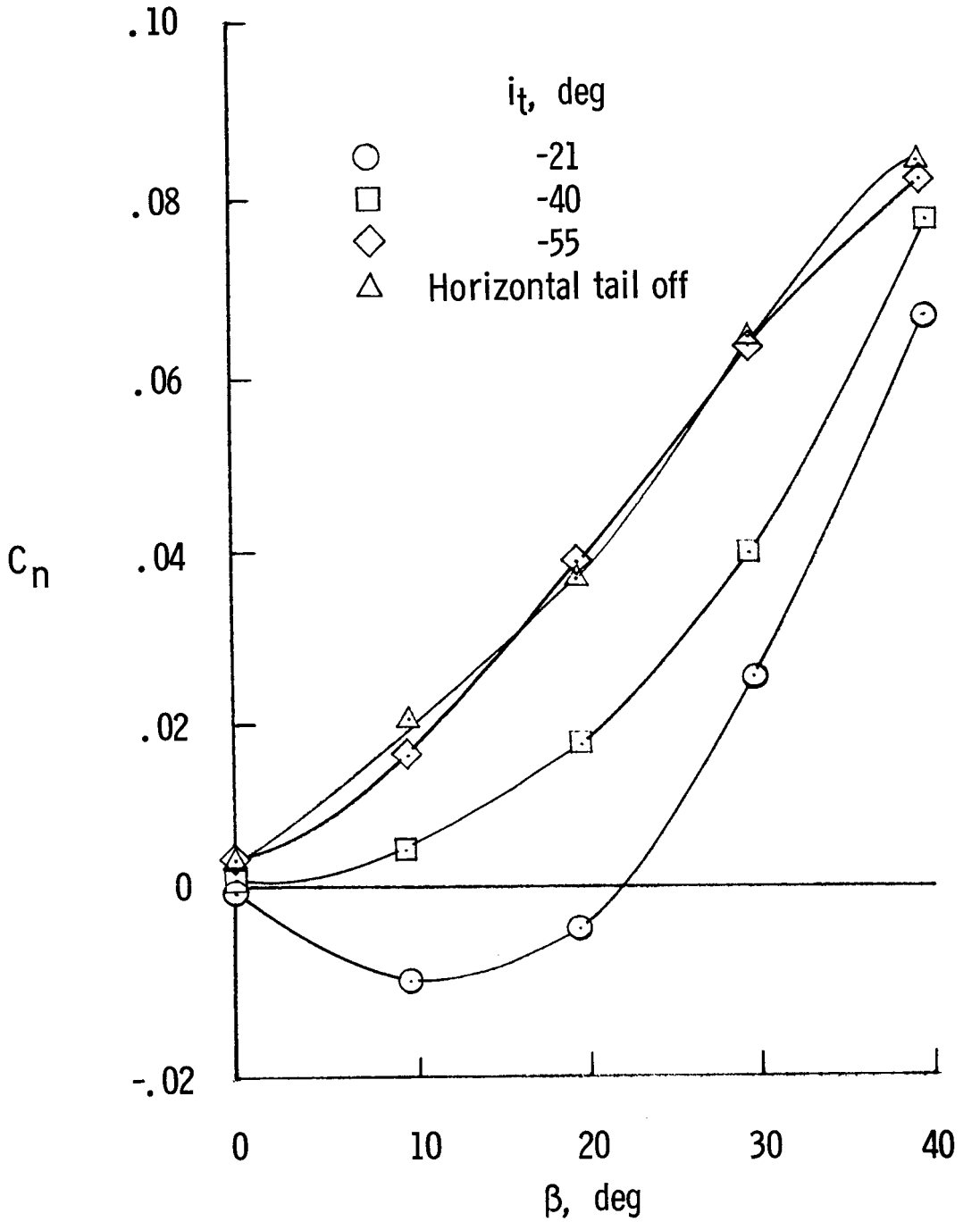

Figure 10.- Effect of horizontal tail incidence angle on yawing-moment characteristics. $\alpha = 85^{0}$.

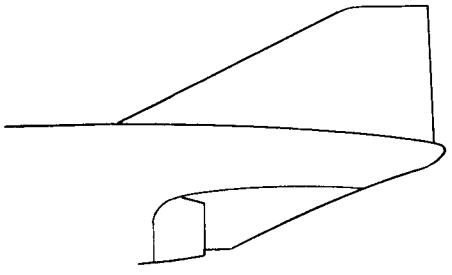

Horizontal tail removed

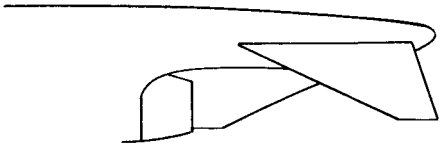

Vertical tail removed

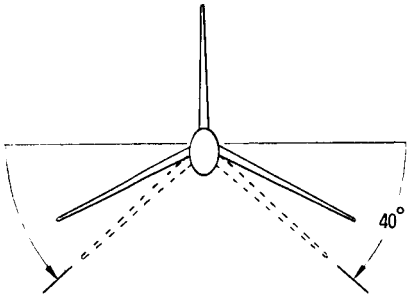

Increased anhedral

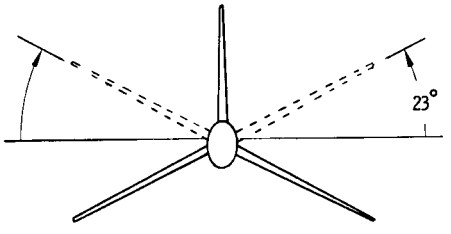

Inverted tail

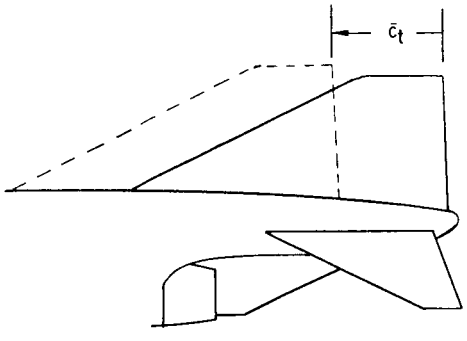

Relocation of vertical tail

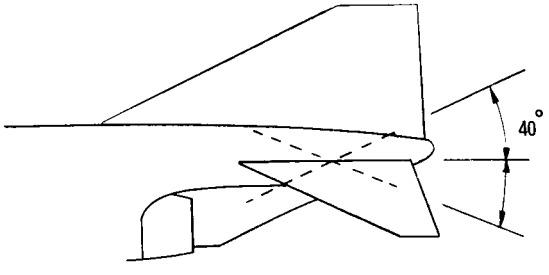

Increased horizontal tail incidence limits

Figure 11.- Tail arrangements studied during autorotation tests.

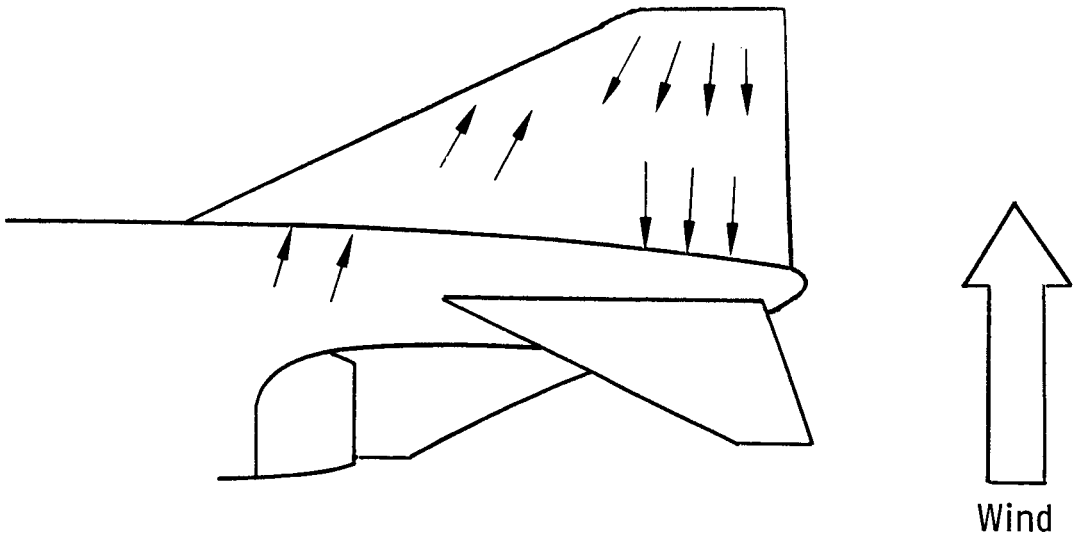

(a) Advancing side.

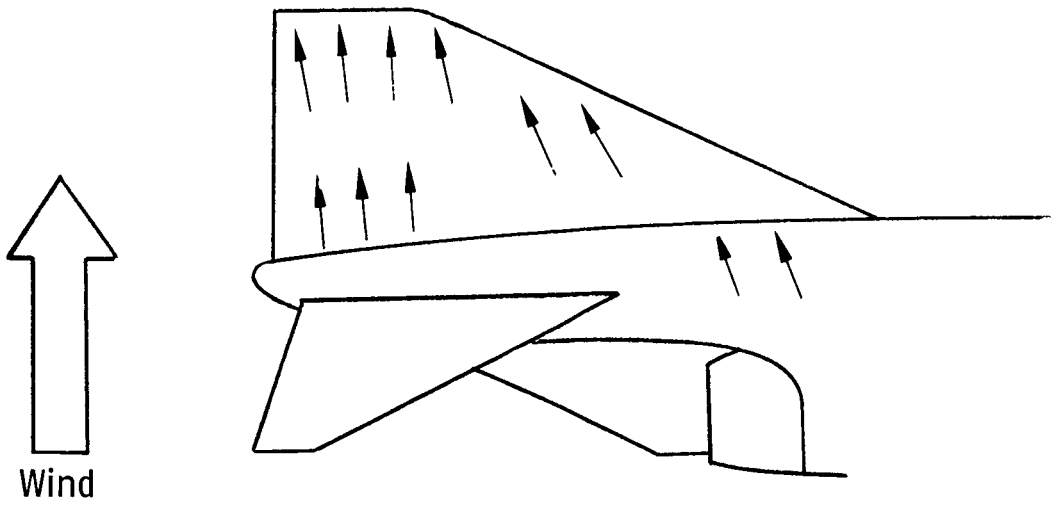

(b) Trailing side.

Figure 12.- Typical tuft patterns on vertical tail surfaces during autorotation (right spin).

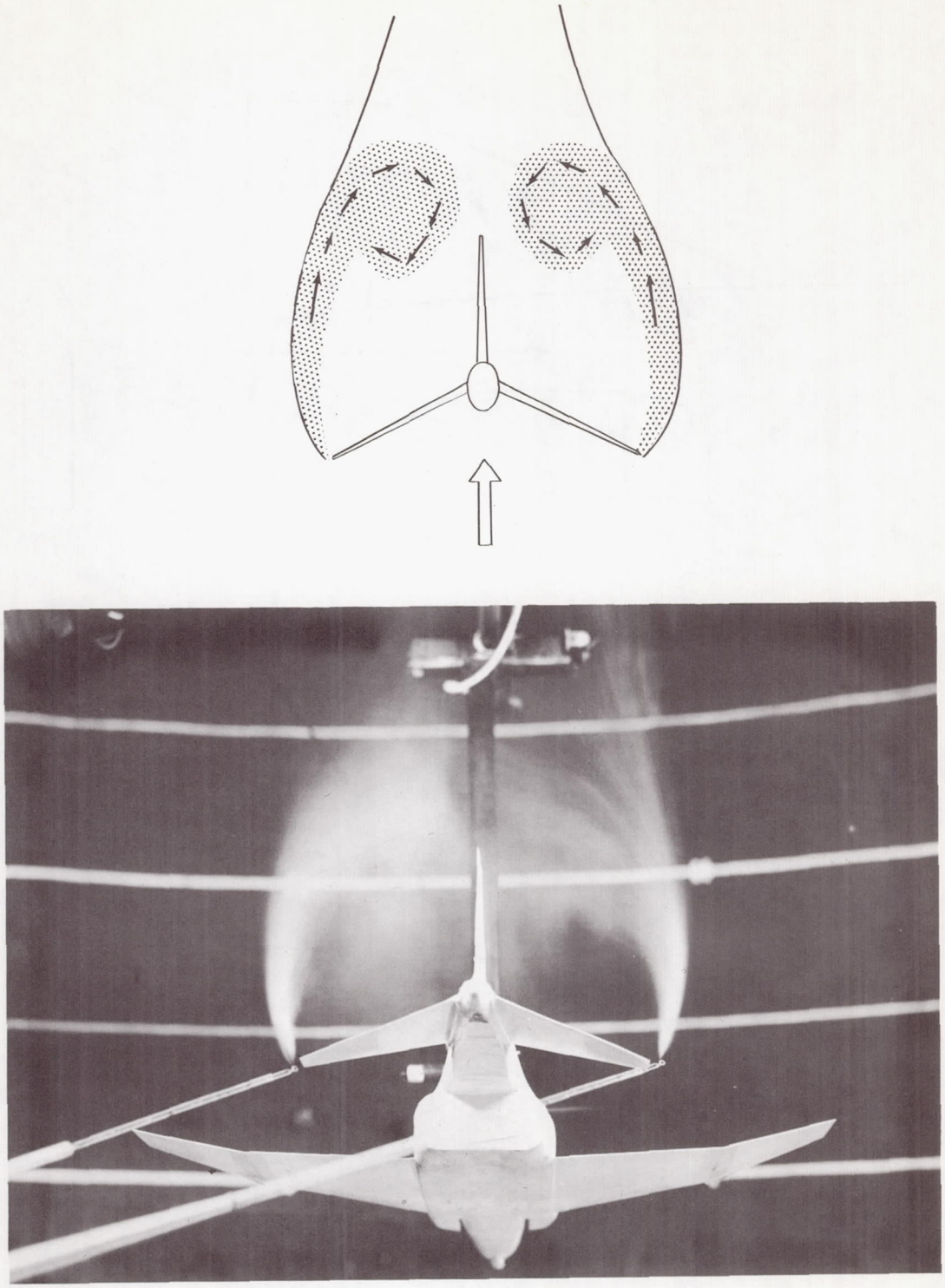

(a) $\beta = 0^{o}$.

L-69-5242

Figure 13.- Typical smoke pattern about rear end of model. $\alpha = 90^{o}$; $i_t = 0^{o}$.

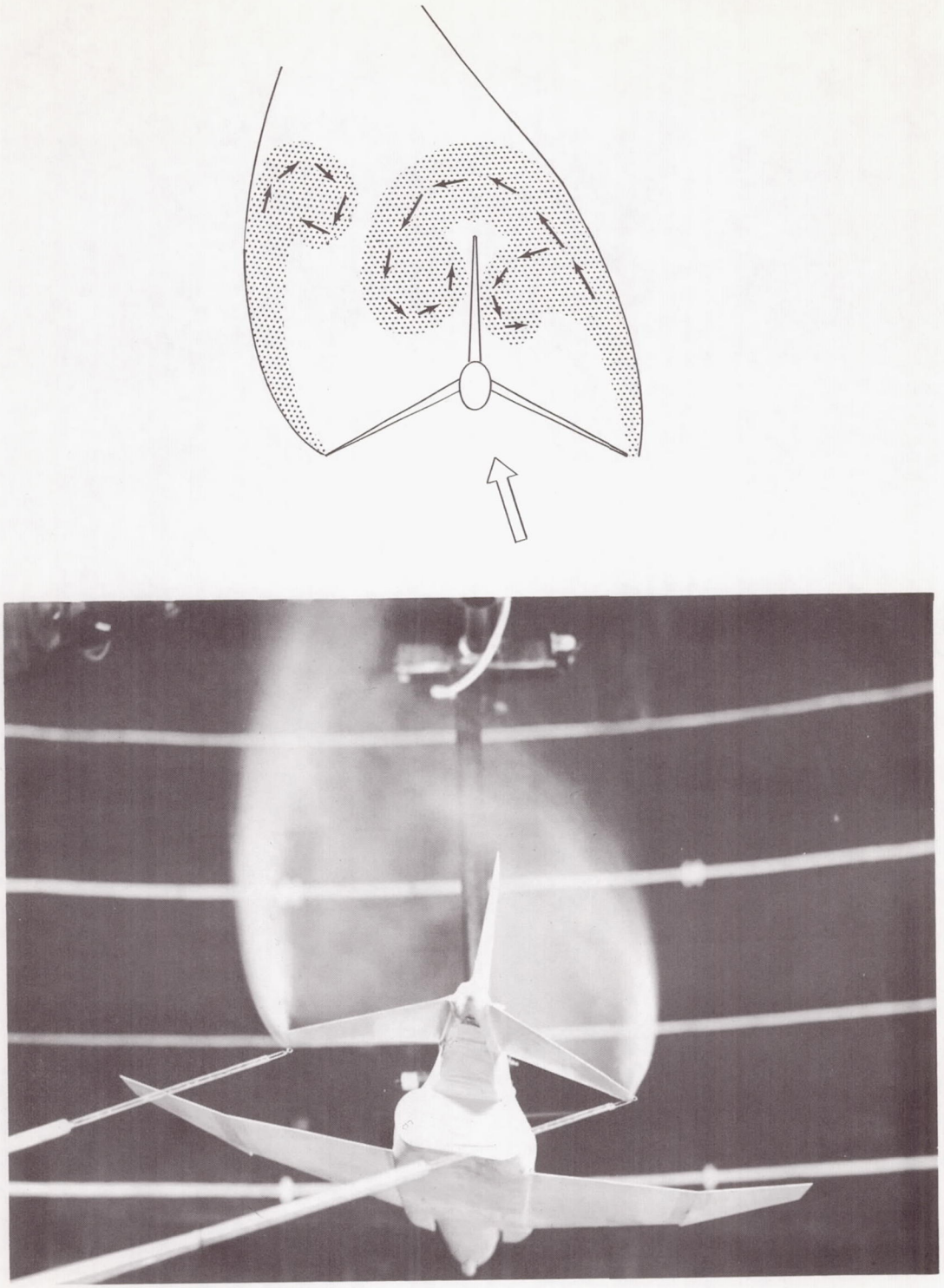

(b) $\beta = 10^{0}$.

L-69-5243

Figure 13.- Concluded.